Geophysical Research Letters

RESEARCH LETTER
10.1029/2022GL102337

Key Points:

- The initiation of the L'Aquila earthquake is characterized by a small amplitude signal before the onset of large amplitude *P*-waves
- We evidence a slow rupture velocity during the rupture initiation of the L'Aquila earthquake
- Low seismic efficiency indicates that most of the energy budget was used to initiate the rupture (fracture energy ~76%)

Supporting Information:

Supporting Information may be found in the online version of this article.

Correspondence to:

L. Cabrera,
leoncio.cabrera@univ-grenoble-alpes.fr

Citation:

Cabrera, L., & Poli, P. (2023). A struggled rupture initiation of the M_w 6.1 2009 L'Aquila earthquake. *Geophysical Research Letters*, *50*, e2022GL102337. https://doi.org/10.1029/2022GL102337

Received 2 DEC 2022
Accepted 11 MAR 2023

A Struggled Rupture Initiation of the M_w 6.1 2009 L'Aquila Earthquake

Leoncio Cabrera[1] and Piero Poli[1,2]

[1]CNRS, ISTerre Institut des Sciences de la Terre, Université Grenoble Alpes, Grenoble, France, [2]Dipartimento di Geoscienze, Università di Padova, Padova, Italy

Abstract Understanding under which physical conditions large earthquakes begin, is a key question in Earth science. Laboratory experiments and numerical models have shown that earthquake nucleation has distinct phases: a quasi-static and an acceleration stage, followed by dynamic propagation. However, obtaining observations of such or similar processes in nature is complex. Here, we report on the rupture initiation of the M_w 6.1 2009 L'Aquila earthquake. From the detailed analysis of seismic waves recorded at several stations, we identify an ~0.6-s signal preceding the large dynamic rupture. From the geometrical characterization and rupture parameters of this initial phase, we infer that the rupture struggled to initiate exhibiting a slow rupture velocity ($Vr = 0.9 \pm 0.2$ km/s) and low seismic efficiency ($\eta = 0.24$) due to a complex environment in the region where the rupture starts. We also show that the parameters of the rupture initiation are representative of scale-dependent quantities for slip-dependent nucleation models.

Plain Language Summary Understanding the process leading to a large earthquake is a key question in Earth science with implications for earthquake prediction and risk assessment. Although results from laboratory experiments and numerical simulations show that earthquake nucleation is composed of several preliminary stages, these stages and the associated processes are very difficult to observe in natural earthquakes. In this work we study the M_w 6.1 2009 L'Aquila earthquake, and show that it started with a slow rupture, where most of the energy was used to propagate the rupture. Our results show that the rupture struggled to initiate, and it did it slowly probably due to the conditions in which it starts. In addition, our results show similarities with previous work done for earthquakes in different regions of the world and also using theoretical models.

1. Introduction

Understanding the physical processes and conditions that lead to the initiation of an earthquake is one of the major challenges of seismology, with implications for earthquake prediction and risk assessment. Therefore, it is crucial to detect and study signals that allow us to relate the rupture of an earthquake to precursory physical processes, if any exist.

Nowadays, we know from laboratory experiments (e.g., Latour et al., 2013; McLaskey, 2019; Ohnaka & Shen, 1999) and numerical models (e.g., Ampuero & Rubin, 2008; Dascalu et al., 2000; Kaneko et al., 2016; Shibazaki & Matsu'ura, 1998) that earthquakes are preceded by different phases: a stable quasi-static deformation phase (phase I), which evolves into an unstable acceleration phase (phase II), after which the large dynamic rupture occurs (phase III). However, direct measurements of the phases I and II in nature are hard, and the scientific community mostly relies on seismological observations, which are perhaps the most informative about the physical processes that precede large earthquakes.

Two of the main types of precursory seismological observations are foreshocks (e.g., Dodge et al., 1996; Bouchon et al., 2011; Ellsworth & Bulut, 2018; Kato et al., 2012; Ruiz et al., 2014, 2017; Sánchez-Reyes et al., 2021; Cabrera et al., 2022 and references therein) and the seismic signals related to the initial part (i.e., over a few seconds or less) of the mainshock waveform, often known as the seismic nucleation phase (e.g., R. Abercrombie & Mori, 1994; R. E. Abercrombie et al., 1995; Beroza & Ellsworth, 1996; Colombelli et al., 2014; Ellsworth & Beroza, 1995, 1998; Kilb & Gomberg, 1999; Iio, 1992; Mori & Kanamori, 1996; Poli et al., 2016; Tape et al., 2018; Umeda, 1990). This initial phase is represented by a small emergent amplitude signal that is sometimes observed before the large impulsive amplitude onset of the *P*-waves (Figure 1). Results from different studies focused on this initial phase have revealed a variety of new insights about the rupture initiation. Umeda (1990)

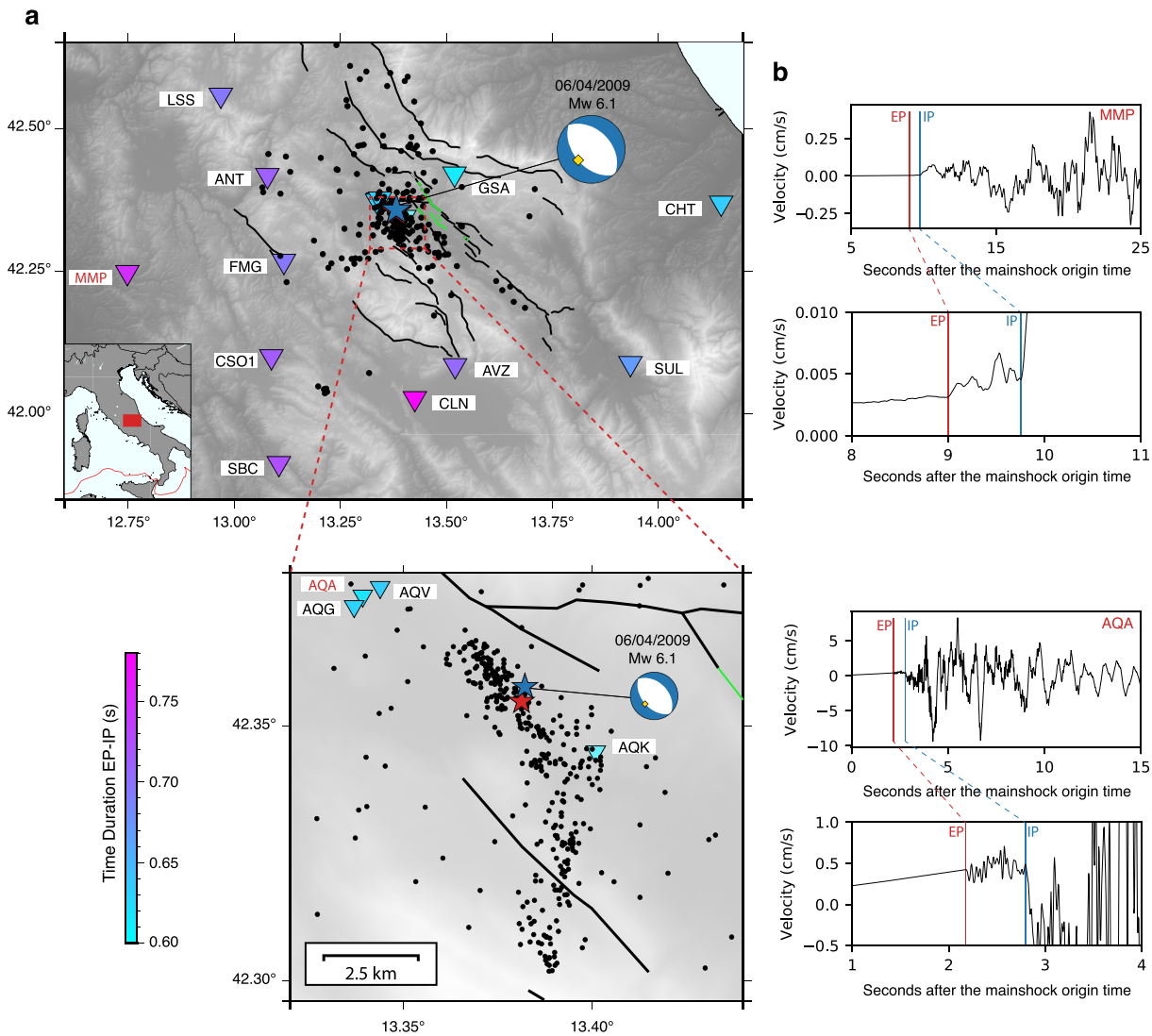

Figure 1. (a) Location map for the L'Aquila earthquake, showing the precursory seismicity (black dots) reported by Chiaraluce et al. (2011), and the strong motion stations (triangles) used in this study. The colors of the triangles indicate the duration between the initial emergent *P*-waves (EP, red star) and the large impulsive onset (IP, blue star) *P*-waves waves located by Di Stefano et al. (2011). Black and green thin lines represent traces of the active mapped faults and co-seismic surface ruptures, respectively (Boncio et al., 2010). Focal mechanism (reported by the Istituto Nazionale di Geofisica e Vulcanologia) for the mainshock and EP (yellow diamond, Table 1). (b) Vertical component velocity seismograms (Luzi et al., 2020) of the initial *P*-waves recorded for stations at different distances from the epicenter. Red and blue vertical lines indicate the arrival times of EP and IP, respectively.

found that the duration of the initial phase increases proportionately with the earthquake size. Iio (1992, 1995) and Iio et al. (1999) showed that the emergent initial phase can be explained by models that predict slow slip velocities and/or rupture velocities immediately after rupture initiation, and that the initial slow phase is not a product of attenuation, but a source effect. Similarly, Shibazaki and Matsu'ura (1998) modeling far-field seismograms showed that the slow initial phase can be radiated in the theoretical acceleration phase (phase II) from the slow growth of a rupture. Using a larger data set of earthquakes, Ellsworth and Beroza (1995) and Beroza and Ellsworth (1996) found that the size and duration of the initial phase scale with the final magnitude. In addition, selected group of earthquakes and seismic sequences have been studied in more detail such as the 1981 Gulf of Corinth earthquake (R. E. Abercrombie et al., 1995), the 1995 Ridgecrest events (Ellsworth & Beroza, 1998; Mori & Kanamori, 1996), the 1994 Northridge California earthquake (Kilb & Gomberg, 1999), intermediate depth events in the Hindu Kunsh nest (Poli et al., 2016) and events in central Alaska (Tape et al., 2018), among others.

On 6 April 2009 the M_w 6.1 L'Aquila earthquake struck central Italy causing damage and fatalities (Chiaraluce et al., 2011; Valoroso et al., 2013). It was preceded by thousands of foreshocks (Cabrera et al., 2022) and an emergent initial phase recorded by near-field accelerometers (Figure 1a, Ellsworth & Chiaraluce, 2009; Di Stefano et al., 2011). In this work we study this initial phase to get new insights into the rupture initiation process of earthquakes. For this aim we take advantage of a dense azimuthal coverage of stations and we derive quantitative parameters (R. E. Abercrombie et al., 2017) of the rupture initiation (Figure 1b). Then, the results are compared with theoretical models (e.g., Ohnaka, 2000) and previous observations (e.g., Beroza & Ellsworth, 1996). We do not analyze the large dynamic rupture after the initial phase, as previous studies have done so (e.g., Atzori et al., 2009; Cheloni et al., 2010; Cirella et al., 2012; Scognamiglio et al., 2010; Trasatti et al., 2011). Our results reveal how the L'Aquila earthquake struggled to begin due to the heterogeneity of the physical properties of the fault, which can be understood in the context of well-known nucleation models (Ampuero & Rubin, 2008; Dascalu et al., 2000; Kaneko et al., 2016; Ohnaka, 2000) as a significantly large slip-weakening distance (Dc).

2. Analysis of the Rupture Initiation

As illustrated in Figure 1b (see also Figure S1 in Supporting Information S1), the seismograms recorded at triggered regional accelerometers (Figure 1a) show a short (~0.6-s) small emergent amplitude signal (Figure 1b, EP), before the onset of large impulsive amplitude *P*-waves (Figure 1b, IP). By locating the hypocenter of both phases (i.e., EP and IP), Di Stefano et al. (2011) interpreted EP as the initial rupture process of the L'Aquila earthquake, and defined it as a seismic nucleation phase (Ellsworth & Beroza, 1995; Ellsworth & Chiaraluce, 2009). In this work we will call this initial phase the rupture initiation.

The rupture initiation keeps on growing from EP until the large amplitude onset (IP). Figure S2 in Supporting Information S1 exemplifies this feature. This behavior is confirmed by comparing the waveforms of the rupture initiation and two M_w 3.9 foreshocks that occurred close to the hypocenter and were recorded at the closest broadband station located right on top of the hypocenters. We here assume that the rupture initiation is one event with duration from EP to IP. At the termination of the rupture, at time IP, the large slip identified by the large amplitude seismic waves onset (IP) is starting, in agreement with other studies (Cirella et al., 2012; Colombelli et al., 2014; Di Stefano et al., 2011; Ellsworth & Beroza, 1995, 1998; Iio, 1992; Poli et al., 2016).

We measure the time duration between EP and IP (t_{EP-IP}) at 15 strong motion stations located in the near field (epicentral distance, <60 km) with good azimuthal coverage (Figure 1; Luzi et al., 2020), for which both EP and IP are clearly registered and easily identified (see examples in Figure 1b and for all of the stations in Figure S1 in Supporting Information S1). For this purpose, we use the raw vertical velocity seismograms from the Engineering Strong Motion Database (ESM) of the Istituto Nazionale di Geofisica e Vulcanologia (INGV) recorded with a sampling rate of 200 Hz (Luzi et al., 2020). This high sampling rate permits to have a time resolution of 0.005 s and allows us to ensure a correct recording of the rupture initiation (Beroza & Ellsworth, 1996). We do not apply any filter, and we manually pick the time arrival for EP and IP (see examples in Figure 1 and Figure S1 in Supporting Information S1). The time t_{EP-IP} as a function of the azimuth, reveals a clear azimuthal variation (Figure 2a), which indicates directivity due to the finiteness of the rupture process (R. E. Abercrombie et al., 2017). Beyond the azimuthal directivity, we further observe how down-going and up-going *P*-waves, that have similar azimuths, have different duration (e.g., see differences for the take-off angles of SUL-AQK and LSS-AQG-AQA-AQV), suggesting a significant vertical component for the rupture initiation (R. E. Abercrombie et al., 2017).

Before proceeding with further analysis, we assess whether the recorded signals and their azimuthal dependence are controlled by propagation effects. For this purpose, we model our observations as a Gaussian pulse of duration 0.6 s (our smallest time measurement, Figure S3 in Supporting Information S1). We then apply an attenuation factor (Anderson & Hough, 1984) for the different travel times, for each station, and test a range of quality factors Q (see Text S1 and Figure S4 in Supporting Information S1). The resulting waveforms (Figure S4 in Supporting Information S1) show a marginal effect of attenuation on the waveform shape and related duration, thus supporting the robustness of our azimuthal measures (Figure 2a). The analysis of attenuation effects also reveals that our time measurements (≥0.6 s) are systematically larger than potential attenuation effects, and can thus be used to infer rupture properties. This is in concordance with the work done by Iio et al. (1999) who showed that the rupture initiation does not arise from the attenuation, but is a source effect. In addition, according to Beroza and Ellsworth (1996) for $M > 4.0$ earthquakes, the duration of this rupture initiation should be greater than ~0.3 s (considering their proposed scaling) and the attenuation should not have any role (Beroza

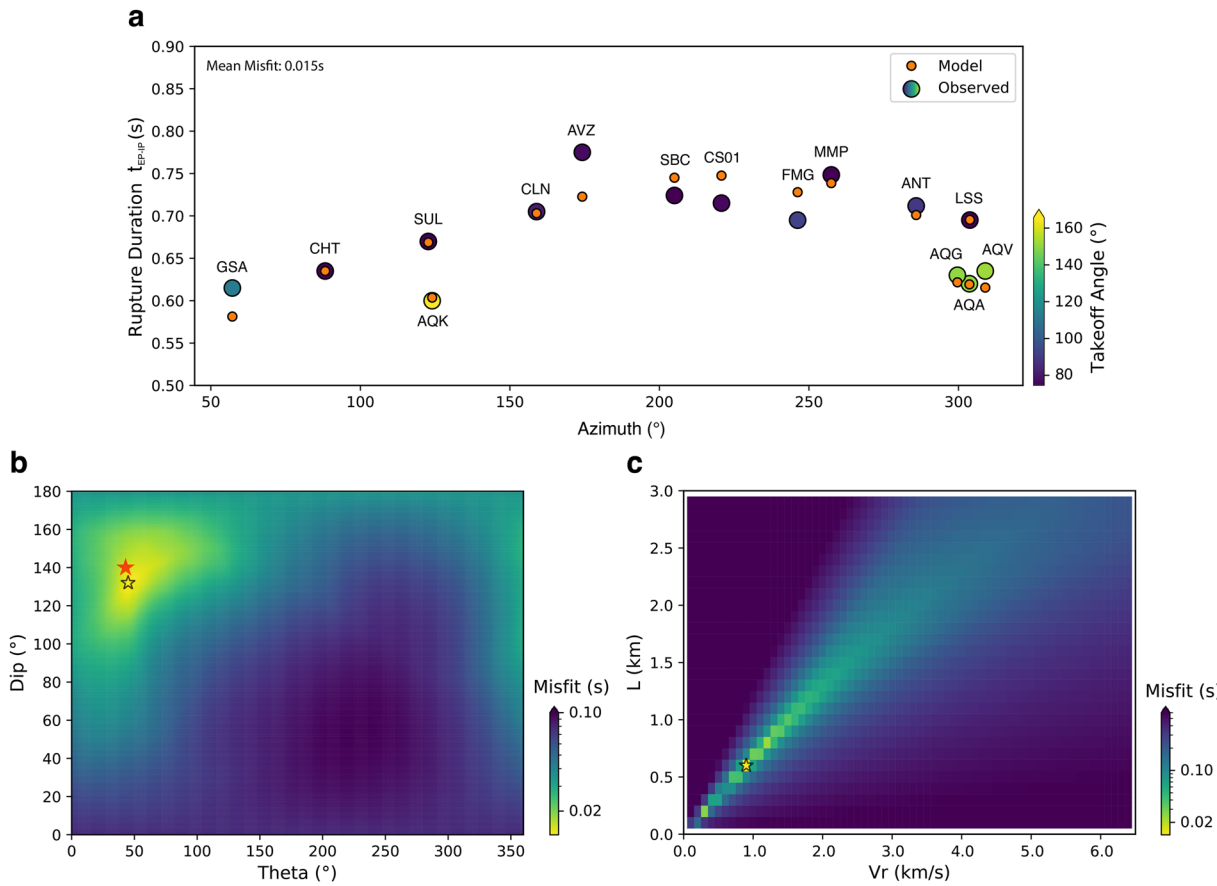

Figure 2. Observations, best model and misfit. (a) Observed rupture times t_{EP-IP} (colored according to the take-off angle) as a function of the azimuth compared with the best solution synthetics (orange dots). (b) Misfit between the dip of the rupture initiation (i.e., 0° = vertically down, 90° = horizontal, and 180° = vertically up) as a function of the strike of the rupture initiation. The black star contour indicates the minimum misfit and the red star indicates the dip and an angle perpendicular to the strike of the fault system (50° and N47°E, respectively according to Chiaraluce et al., 2011). (c) Misfit between the length of the linear source as a function of the rupture velocity. The black star contour indicates the minimum misfit.

& Ellsworth, 1996). Furthermore, we ruled out the existence of other seismic phases by modeling their arrival time using a local velocity model (Chiaraluce et al., 2011) and the ObsPy TauP Toolkit (Beyreuther et al., 2010; Crotwell et al., 1999). Figure S5 in Supporting Information S1 shows that the times observed for IP do not correspond to any other phase arrival.

We finally quantitatively study the rupture initiation in terms of its geometry (i.e., rupture plane orientation and rupture velocity), and estimate some rupture parameters.

Table 1
Parameters Retrieved for the Rupture Initiation Considering a Line Source Model

Parameter	Value	Searching space	Grid search step
θ (°)	45 ± 5.0	$0 - 360$	1
δ (°)	132 ± 5.0	$0 - 180$	1
Vr (km/s)	0.9 ± 0.2	$0 - Vp$	0.1
L (km)	0.6 ± 0.1	$0 - 3$	0.1
$Misfit$ (s)	0.015 ± 0.002		

2.1. Geometry of the Rupture Initiation

To retrieve the geometry of the rupture initiation (i.e., first ~0.6 s of the signal), we use an approach that takes advantage of the azimuthal variation in the seismic radiation (i.e., directivity) and that has been used to analyze small earthquakes (R. E. Abercrombie et al., 2017). Our main assumption is that the rupture can be represented by a line kinematic source model with uniform slip and constant rupture velocity. This model, although simplified, has shown good results in the study of small earthquakes in which kinematic inversions using heterogeneous models to account for high frequencies are not plausible (e.g., R. E. Abercrombie et al., 2017). In addition, considering a line source model facilitates comparison with theoretical parameters such as the critical rupture length (Lc, Ohnaka, 2000. See discussion section).

Following R. E. Abercrombie et al. (2017), the rupture duration (T) at station i given a line source of size L is given by

$$T_i = L/Vr(1 - \cos\theta_i \sin\phi_i \sin\delta Vr/V - \cos\phi_i \cos\delta Vr/V) \quad (1)$$

where Vr is the rupture velocity, V is the P- (Vp) or S- (Vs) wave velocity at the source, ϕ_i is the take-off angle, and θ_i and δ are the azimuth and dip of the rupture direction, respectively (the take-off angles and the dip are defined as 0° = vertically down, 90° = horizontal, and 180° = vertically up). We use Vp = 6.5 km/s, based on a local three-dimensional tomographic model (Di Stefano et al., 2011). The take-off angles are calculated using the ObsPy TauP Toolkit (Beyreuther et al., 2010; Crotwell et al., 1999) in a local velocity model (Chiaraluce et al., 2011) considering the EP hypocenter previously estimated by Di Stefano et al. (2011). Then, assuming $T_i = t_{EP-IP}$ in Equation 1, we use a grid search procedure to estimate the Vr, L, θ, and δ that best explain the observations minimizing an $L1$ norm (R. E. Abercrombie et al., 2017). In addition, the grid search is repeated 1,000 times, randomly removing two stations each time. The result is stored every time, and the ensemble of the measures is used to evaluate the uncertainty of the estimates.

Table 1 shows a summary of the results. The estimated strike (θ) and dip (δ) of the rupture initiation are, respectively, 45° ± 5.0° and 132° ± 5.0° (where dip is defined as 0° = vertically down, 90° = horizontal, and 180° = vertically up), which indicates a north-east initial rupture perpendicular to the fault system (N137°E, Chiaraluce et al., 2011) and going upwards, in agreement with the dip of the fault system of ∼50° (Chiaraluce et al., 2011; Figure 2a), kinematics models (e.g., Cirella et al., 2012) and absolute locations of EP and IP (Figure 1, Di Stefano et al., 2011). Our estimated strike and dip of the rupture initiation are also consistent with the focal mechanism reported by the INGV for the mainshock (Figure 1), which indicates that the geometry of the rupture initiation is similar to the geometry of the large dynamic rupture. We also corroborate the relative geometry by relocating EP and IP using the Growclust software (Trugman & Shearer, 2017). For this purpose, we considered all the measured t_{EP-IP} values at the strong motion stations (Figure 1) as the differential delay times and a local velocity model (Chiaraluce et al., 2011). In addition, we performed two tests considering different initial locations for EP and IP, and another test considering the same initial location for EP and IP (see details in Text S2 and Table S1 in Supporting Information S1). In both cases, the geometries retrieved from the relocation indicate a north-east and upwards propagating rupture (see Tables S2 and S3 in Supporting Information S1), supporting the robustness of our estimations.

Our results also indicate a relatively slow rupture velocity (Vr) of 0.9 ± 0.2 km/s and a linear rupture length (L) of 0.6 ± 0.1 km for the rupture initiation. Assuming a constant rupture velocity, the duration of the rupture initiation is ∼0.66 s (we discuss more in detail in the discussion section). Our slow rupture velocity is in agreement with an initial region of lower rupture velocity around EP reported by Cirella et al. (2012). Di Stefano et al. (2011) estimated a larger rupture velocity for EP (∼2.2 km/s) from a 2 km rupture between EP and IP using absolute locations. However, absolute locations are less sensitive to the relative geometry between EP and IP. Our relative relocation using GrowClust estimates a distance ∼500 m in agreement with L (see Tables S2 and S3 in Supporting Information S1).

Figures 2b and 2c shows the misfit between the dip of the rupture initiation as a function of the strike of the rupture initiation and the length of the line source as a function of the rupture velocity. Clear minima are observed in both plots, as well as in those that relate the rest of the parameters (Figure S6 in Supporting Information S1), which illustrates the robustness of our estimates. In addition, Figure 2a shows the comparison of the best solution synthetics and the observed rupture times as a function of the azimuth. Remarkably, our solution can reproduce rupture times (t_{EP-IP}) for stations that have azimuths in common but different take-off angles (e.g., stations SUL-AQK and LSS-AQG-AQA-AQV) with a misfit of 0.015 s. This implies that we can reproduce the observed up-going and down-going P-waves, and that the estimate of the dip is therefore robust.

2.2. Magnitude of the Rupture Initiation

To estimate the magnitude of the EP, we follow Peng and Zhao (2009) and we compare the maximum amplitudes of the EP waveform with that of foreshock events within a three-dimensional radius of 500 m, where the M_w is reported in a local seismic catalog (Chiaraluce et al., 2011). This procedure is more suitable than using the spectrum of the waveforms, as the time window of the signals is very short and they have a non-zero base-line (see Madariaga et al., 2019).

Since the strong motion records correspond to a trigger system that is activated when a certain acceleration threshold is exceeded, there are no foreshocks recorded for the stations shown in Figure 1. Therefore, we use the four closest broadband stations (See Figure S7a in Supporting Information S1; INGV Seismological Data Centre, 2006; MedNet Project Partner Institutions, 1990), for which the EP and IP identification is straightforward, and extract their waveform after detrending and applying a high-pass filter (0.6 Hz) to the raw seismograms. Thus, we compute the magnitude of EP based on the mean value of the maximum amplitude ratios for all the vertical channels between the foreshocks and EP, assuming that a ratio of 10 in the amplitude ratios corresponds to a variation of one-unit of magnitude (e.g., Cabrera et al., 2021, 2022; Essing & Poli, 2022; Frank et al., 2017; Peng & Zhao, 2009). We perform the same procedure for 11 foreshocks (Figure S7a in Supporting Information S1) considering a time window identical to $t_{\mathrm{EP-IP}}$ at the corresponding station and starting at the *P*-wave arrival. The selected time window is long enough to capture the foreshocks *P*-waves, and at the same time short enough to avoid interfering with the *S*-wave signals (see e.g., Figure S2b in Supporting Information S1). It is important to note that, although the broadband seismic records are clipped shortly after the onset of IP for the mainshock, they are not between EP-IP (see Figure S9 in Supporting Information S1). We obtain a magnitude of 3.99 ± 0.18 for EP (see Figure S7b in Supporting Information S1). The robustness of our estimation is observed in Figure S2b in Supporting Information S1, which shows the comparison between the raw waveforms of EP-IP and two M_{w} 3.9 foreshocks that occurred 1 week and 5 hr before the mainshock. We note that although their amplitudes are similar, the amplitude of EP grows with time until the onset of IP (Figures S1 and S2 in Supporting Information S1). We also validated our methodology by estimating the magnitude of a foreshock of known magnitude (see Figure S8 in Supporting Information S1) and using spectral approaches (e.g., Walter et al., 2017). Thus, the seismic moment (Mo) of the rupture initiation is 1.23×10^{15} Nm, which corresponds to ~0.07% of the mainshock seismic moment (see more detail below).

2.3. Rupture Parameters of the Rupture Initiation

In this section we use the measures obtained above (Vr, L, and Mo) to derive some rupture parameters of the rupture initiation. We assume a circular shear crack model with spatially constant stress drop, having a radius (r) of 300 m (L/2) and a shear modulus (μ) of 30 GPa. Although a circular crack model may appear simplified, its adoption is reasonable given the small magnitude of the rupture initiation (Section 2.2). Moreover, this model makes our results directly comparable with studies on conventional earthquakes (e.g., Venkataraman & Kanamori, 2004) and previous observations of seismic nucleation phases (Beroza & Ellsworth, 1996).

The average slip and the stress drop are estimated as $\Delta u = \frac{Mo}{\mu \pi r^2}$ (Beroza & Ellsworth, 1996) and $\Delta\sigma = \frac{7Mo}{16r^3}$ (Eshelby, 1957), respectively. Our estimations indicate an average slip of 0.15 m which is in agreement with the slip estimated by Cirella et al. (2012) for the region where the rupture begins and a stress drop of 19.9 MPa. Figure S10 in Supporting Information S1 shows that the estimated rupture parameters for the rupture initiation are in agreement with the scaling that relates seismic nucleation phases and their subsequent mainshocks proposed by Beroza and Ellsworth (1996). In addition, Figure S10 in Supporting Information S1 shows that the seismic moment of the rupture initiation is 0.01%–10% of the seismic moment of the mainshock, in agreement with previous studies (Beroza & Ellsworth, 1996; Poli et al., 2016).

Beyond the rupture parameters discussed above, we use the measured rupture velocity (Table 1) to infer the seismic efficiency (η), assuming a crack model with constant rupture velocity (Husseini & Randall, 1976; Kanamori et al., 1998):

$$\eta = 1 - \sqrt{\frac{\beta - Vr}{\beta + Vr}} \tag{2}$$

η describes the proportion of the total energy radiated as seismic waves. If $\eta = 1$, the rupture is very efficient in radiating energy. If $\eta = 0$, the entire energy is dissipated mechanically and no energy is radiated (see Kanamori, 2004). Thus, considering a shear wave velocity (β) of 3,300 m/s, according to a local velocity model (Chiaraluce et al., 2011), we obtain $\eta = 0.24$ for the rupture initiation, which implies that nearly 80% of the energy was dissipated during the initial rupture.

We now combine the stress drop ($\Delta\sigma$) with the seismic efficiency (η) to estimate the total energy (E_T), fracture energy (E_G) and energy density (G') using the expressions derived by Eshelby (1957) and Poli and Prieto (2016)

for a circular shear crack model of constant stress drop. G' is especially useful because it allows us to compare our results with values of G' as a function of Δu estimated from laboratory experiments, geological observations, modeling and seismological observations (for a review see Cocco et al., 2023):

$$E_T = \frac{8}{7}\frac{\Delta\sigma^2}{\mu}r^3 \tag{3}$$

$$E_G = E_T(1-\eta) \tag{4}$$

Assuming $\mu = 30\,\text{GPa}$ and $\eta = 0.24$, we obtain $E_T = 4.09 \times 10^{11}$ J and $E_G = 3.09 \times 10^{11}$ J. Finally, assuming that the fracture energy rate does not vary on the fault area we can estimate the fracture energy density (G') as:

$$G' = \frac{8}{7}\frac{\Delta\sigma^2}{\pi\mu}r(1-\eta) \tag{5}$$

We estimate $G' = 1.09 \times 10^6$ J/m^2 for the rupture initiation. This corresponds to the upper bound of previous estimated values of G' for events with an average slip of 0.15 m (see a compilation in Cocco et al., 2023), which is explained by the higher percentage of the energy budget associated with fracture energy during the initiation rupture.

3. Discussions

The M_w 6.1 2009 L'Aquila earthquake started with a ∼0.6-s small amplitude rupture (∼0.07% of the total moment), which preceded the large dynamic rupture (Figure 1). From our geometrical analysis, we infer that the rupture initiation occurred in the fault plane where the large dynamic rupture takes place.

The inferred parameters for the rupture initiation (duration, r, Mo, Δu) follow the scaling observed in previous studies (Beroza & Ellsworth, 1996; Colombelli et al., 2014; Iio, 1992; Poli et al., 2016; Figure S10 in Supporting Information S1), which suggests that scale-dependent quantities control the underlying physics of earthquake initiation (Ohnaka, 2000).

Beyond the well-studied parameters for rupture initiation (e.g., Beroza & Ellsworth, 1996; Colombelli et al., 2014; Iio, 1992; Poli et al., 2016, Figure S10 in Supporting Information S1), we also estimate the rupture velocity (Table 1). The inferred rupture velocity ($Vr = 0.9 \pm 0.2$ km/s) is slower than that of ordinary crustal earthquakes. For instance, considering $\beta = 3,300$ m/s (Chiaraluce et al., 2011), we obtain $Vr/\beta = 0.27$. This value contrasts with the $Vr/\beta = 0.7 - 0.8$ usually observed for crustal earthquakes (Kanamori et al., 1998). However, Vr is on the order of the estimated rupture velocities for tsunami earthquakes, which are about 1.0 km/s (e.g., Bryant, 2008; Fujii & Satake, 2007). These slow rupture velocities for tsunami earthquakes led to greater directivity (Bryant, 2008), as we here observe for the rupture initiation (Figures 1 and 2). Since tsunami earthquakes mainly occur at subduction zones, the slower rupture velocities have been associated to anomalous elastic properties of the uppermost part of the subduction zone, where a complex accretionary wedge is developed in the hanging wall of the megathrust (Sallarès & Ranero, 2019).

Furthermore, our estimated seismic efficiency ($\eta = 0.24$) indicates an ineffective rupture initiation in terms of radiated seismic energy. Venkataraman and Kanamori (2004) compiled observations for several subduction zone earthquakes, and show that most earthquakes have seismic efficiencies in the range 0.25–1. By contrast, tsunami earthquakes and some deep earthquakes have very small seismic efficiencies (<0.25) and hence dissipate a large amount of energy during faulting. Venkataraman and Kanamori (2004) proposed that low seismic efficiency for shallow megathrust earthquakes is a marker of complex rheology near the trench.

The low efficiency for the initial rupture implies a significant amount of fracture energy ($E_G \sim 80\%$ of total energy). This latter is indicative of a large slip-weakening distance (Dc, Beeler et al., 2006; Poli & Prieto, 2016). The large E_G (and thus large Dc) is known to be the main parameter that controls the occurrence of small precursory phases in numerical models (Lapusta & Rice, 2003). The large Dc is also indicative of significant heterogeneity of fault physical properties (Lapusta & Rice, 2003; Ohnaka, 2000; Scuderi & Collettini, 2016).

The ensemble of our parameters indicates a high level of complexity during rupture initiation, which results in a slow rupture velocity and associated low seismic efficiency. One factor controlling this complexity could

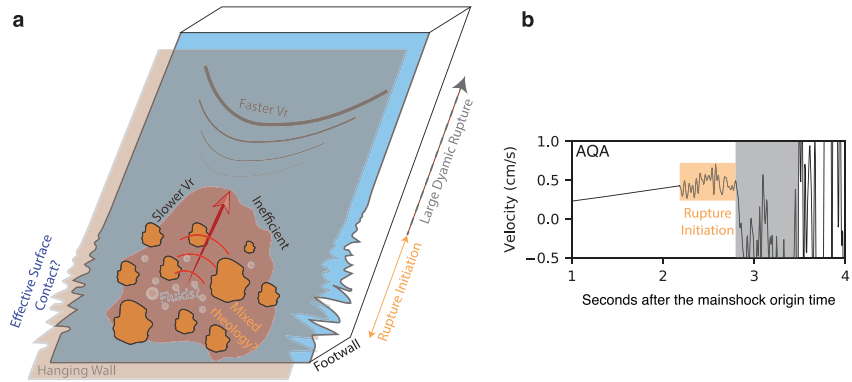

Figure 3. Cartoon summarizing our observations and interpretation. (a) The rupture initiates in a complex zone, which hinders its upward propagation and reduces its rupture velocity. This leads to low seismic efficiency, indicating that most of the energy budget corresponds to fracture energy. Some complexities that may influence the zone are the presence of fluids, a mixed rheology (ductile and brittle) and/or variations in the effective contact surface (see the text for more detail). Once the rupture has left this zone (to the faster Vr region), these complexities no longer play an important role. (b) Seismogram of station AQA (Figure 1) showing the record of the rupture initiation and the large dynamic rupture.

be the significant role of fluids reported in the region (Antonioli et al., 2005; Baccheschi et al., 2020; Lucente et al., 2010; Poli et al., 2020; Savage, 2010; Terakawa et al., 2010). This hypothesis is supported by laboratory experiments indicative of decreasing rupture velocity with increasing fluid pressure (Passelègue et al., 2020). Another factor could be the presence of a mixed rheology, with brittle asperities embedded in a ductile environment in the segment where the rupture starts, as proposed by Cabrera et al. (2022) from the study of the foreshocks preceding the mainshock. A third factor, somehow linked with our second hypothesis, that could play a significant role, is the effective contact surface on the fault. Although it is not possible to measure this parameter directly on the fault, sliding laboratory experiments using two brittle acrylic blocks separated by a rough interface (e.g., Gvirtzman & Fineberg, 2021, 2023; Rubinstein et al., 2004) have shown that dynamic ruptures (i.e., laboratory earthquakes) are preceded by slow rupture fronts that gradually reduce the contact surface until sliding occurs. Considering our observations and the factors described above, our interpretation of the rupture initiation of the L'Aquila earthquake is summarized in Figure 3.

Finally, if we assume that the initial rupture tracks the local physical properties of the earthquake's initiation region, are our derived rupture parameters representative of the energy balance of the rupture initiation for slip-depend models (Ohnaka, 2000)?. Beyond the observed slow Vr (Table 1), which is predicted for initial rupture stage (Ohnaka, 2000), we note that the measured $\Delta\sigma$ (~20 MPa) is in the order of the breakdown stress estimated by Ohnaka (2000) (1–100 Mpa). Furthermore, using the scaling relationships proposed by Ohnaka (2000) for slip-depend models we can estimate the respective Dc and critical nucleation length (2Lc) associated with a M_w 6.1 mainshock (Note that Ohnaka calls 2Lc what we and other authors call Lc, i.e., the critical nucleation length, e.g., McLaskey, 2019). Namely, Ohnaka (2000) proposes $2Lc = \sqrt[3]{Mo}/10^3$ and $Dc = \sqrt[3]{Mo}/10^{19/3}$, where Mo represents the seismic moment of the mainshock. Thus, our estimated average slip and rupture size (Table 1) are relatively on the same order as $Dc = 0.6$ m and $2Lc = 1216$ m estimated from Ohnaka (2000). We thus propose that the derived rupture parameters from the detailed analysis of the initial rupture stage of the L'Aquila earthquake are closely related to scale-dependent quantities of slip-dependent nucleation models.

4. Conclusion

Our full characterization of the rupture initiation including geometry, rupture velocity, and some other rupture parameters reveals important new insights about earthquake initiation, and helps to bridge the gap between laboratory experiments (Latour et al., 2013; McLaskey, 2019), numerical modeling (Kaneko et al., 2016), theoretical studies (Ampuero & Rubin, 2008; Ohnaka, 2000) and observations of faults in nature.

We show that the L'Aquila earthquake started with a slow and seismically inefficient rupture initiation, akin to what is observed for tsunami earthquakes in complex media. The slow seismic efficiency implies a large fracture energy and thus large Dc, which is also indicative of significant heterogeneity in the fault. Based on the results

listed above, we interpret the rupture initiation takes place in a complex environment, where factors such as the presence of fluids, a mixed rheology and the effective contact surface play a key role. In addition, our approach considering a line kinematic source model, although simplified, provides a new opportunity to compare the rupture length and average slip of the rupture initiation with theoretical parameters such as the critical rupture length (Lc) and slip-weakening distance (Dc), indicating that the formers are closely related to scale-dependent quantities of slip-dependent nucleation models.

As we show here, further studies of large earthquakes recorded in the near field, as well as the study of smaller earthquakes could open up new and novel opportunities on how an earthquake starts.

Data Availability Statement

Data was downloaded from the Engineering Strong Motion Database (ESM) of the Istituto Nazionale di Geofisica e Vulcanologia (Luzi et al., 2020). Once in the webpage https://esm-db.eu/#/home (last accessed 2 December 2022), navigate to the "Events" section and choose the L'Aquila earthquake (ESM IDIT-1980-0012). Waveforms can be downloaded from the "Records" section. Computations were performed using the facilities of the University of Grenoble Alpes (UGA) High-Performance Computing infrastructures CIMENT (https://ciment.univ-grenoble-alpes.fr/wiki-pub/index.php/Welcome_to_the_CIMENT_site!). Access to the cluster requires registration by the UGA.

Acknowledgments
LC and PP were supported by the European Union Horizon 2020 Research and Innovation Programme (grant agreements, 802777-MONIFAULTS). We also thank the Editor Germán Prieto and two anonymous reviewers who helped to improve the manuscript.

References

Abercrombie, R., & Mori, J. (1994). Local observations of the onset of a large earthquake: 28 June 1992 Landers, California. *Bulletin of the Seismological Society of America*, *84*(3), 725–734.

Abercrombie, R. E., Main, I. G., Douglas, A., & Burton, P. W. (1995). The nucleation and rupture process of the 1981 Gulf of Corinth earthquakes from deconvolved broad-band data. *Geophysical Journal International*, *120*(2), 393–405. https://doi.org/10.1111/j.1365-246x.1995.tb01827.x

Abercrombie, R. E., Poli, P., & Bannister, S. (2017). Earthquake directivity, orientation, and stress drop within the subducting plate at the Hikurangi margin, New Zealand. *Journal of Geophysical Research: Solid Earth*, *122*(12), 10–176. https://doi.org/10.1002/2017jb014935

Ampuero, J. P., & Rubin, A. M. (2008). Earthquake nucleation on rate and state faults–Aging and slip laws. *Journal of Geophysical Research*, *113*(B1), B01302. https://doi.org/10.1029/2007jb005082

Anderson, J. G., & Hough, S. E. (1984). A model for the shape of the Fourier amplitude spectrum of acceleration at high frequencies. *Bulletin of the Seismological Society of America*, *74*(5), 1969–1993.

Antonioli, A., Piccinini, D., Chiaraluce, L., & Cocco, M. (2005). Fluid flow and seismicity pattern: Evidence from the 1997 Umbria-Marche (central Italy) seismic sequence. *Geophysical Research Letters*, *32*(10), L10311. https://doi.org/10.1029/2004gl022256

Atzori, S., Hunstad, I., Chini, M., Salvi, S., Tolomei, C., Bignami, C., et al. (2009). Finite fault inversion of DInSAR coseismic displacement of the 2009 L'Aquila earthquake (central Italy). *Geophysical Research Letters*, *36*(15), L15305. https://doi.org/10.1029/2009gl039293

Baccheschi, P., De Gori, P., Villani, F., Trippetta, F., & Chiarabba, C. (2020). The preparatory phase of the M_w 6.1 2009 L'Aquila (Italy) normal faulting earthquake traced by foreshock time-lapse tomography. *Geology*, *48*(1), 49–55. https://doi.org/10.1130/g46618.1

Beeler, N. M., Abercrombie, R., & McGarr, A. (2006). Inferring earthquake source properties from laboratory observations and the scope of lab contributions to source physics. *Geophysical Monograph-American Geophysical Union*, *170*, 99.

Beroza, G. C., & Ellsworth, W. L. (1996). Properties of the seismic nucleation phase. *Tectonophysics*, *261*(1–3), 209–227. https://doi.org/10.1016/0040-1951(96)00067-4

Beyreuther, M., Barsch, R., Krischer, L., Megies, T., Behr, Y., & Wassermann, J. (2010). ObsPy: A Python toolbox for seismology. *Seismological Research Letters*, *81*(3), 530–533. https://doi.org/10.1785/gssrl.81.3.530

Boncio, P., Pizzi, A., Brozzetti, F., Pomposo, G., Lavecchia, G., Di Naccio, D., & Ferrarini, F. (2010). Coseismic ground deformation of the 6 April 2009 L'Aquila earthquake (central Italy, M_w 6. 3). *Geophysical Research Letters*, *37*(6), L06308. https://doi.org/10.1029/2010gl042807

Bouchon, M., Karabulut, H., Aktar, M., Özalaybey, S., Schmittbuhl, J., & Bouin, M. P. (2011). Extended nucleation of the 1999 M_w 7.6 Izmit earthquake. *Science*, *331*(6019), 877–880. https://doi.org/10.1126/science.1197341

Bryant, E. (2008). *The underrated hazard*. Springer.

Cabrera, L., Poli, P., & Frank, W. B. (2022). Tracking the spatio-temporal evolution of foreshocks preceding the M_w 6.1 2009 L'Aquila Earthquake. *Journal of Geophysical Research: Solid Earth*, *127*(3), e2021JB023888. https://doi.org/10.1029/2021jb023888

Cabrera, L., Ruiz, S., Poli, P., Contreras-Reyes, E., Osses, A., & Mancini, R. (2021). Northern Chile intermediate-depth earthquakes controlled by plate hydration. *Geophysical Journal International*, *226*(1), 78–90. https://doi.org/10.1093/gji/ggaa565

Cheloni, D., D'agostino, N., D'anastasio, E., Avallone, A., Mantenuto, S., Giuliani, R., et al. (2010). Coseismic and initial post-seismic slip of the 2009 M_w 6.3 L'Aquila earthquake, Italy, from GPS measurements. *Geophysical Journal International*, *181*(3), 1539–1546. https://doi.org/10.1111/j.1365-246x.2010.04584.x

Chiaraluce, L., Valoroso, L., Piccinini, D., Di Stefano, R., & De Gori, P. (2011). The anatomy of the 2009 L'Aquila normal fault system (central Italy) imaged by high resolution foreshock and aftershock locations. *Journal of Geophysical Research*, *116*(B12), B12311. https://doi.org/10.1029/2011jb008352

Cirella, A., Piatanesi, A., Tinti, E., Chini, M., & Cocco, M. (2012). Complexity of the rupture process during the 2009 L'Aquila, Italy, earthquake. *Geophysical Journal International*, *190*(1), 607–621. https://doi.org/10.1111/j.1365-246x.2012.05505.x

Cocco, M., Aretusini, S., Cornelio, C., Nielsen, S. B., Spagnuolo, E., Tinti, E., & Di Toro, G. (2023). Fracture energy and breakdown work during earthquakes. *Annual Review of Earth and Planetary Sciences*, *51*(1), 100304. https://doi.org/10.1146/annurev-earth-071822-100304

Colombelli, S., Zollo, A., Festa, G., & Picozzi, M. (2014). Evidence for a difference in rupture initiation between small and large earthquakes. *Nature Communications*, *5*(1), 1–5. https://doi.org/10.1038/ncomms4958

Crotwell, H. P., Owens, T. J., & Ritsema, J. (1999). The TauP Toolkit: Flexible seismic travel-time and ray-path utilities. *Seismological Research Letters*, *70*(2), 154–160. https://doi.org/10.1785/gssrl.70.2.154

Dascalu, C., Ionescu, I. R., & Campillo, M. (2000). Fault finiteness and initiation of dynamic shear instability. *Earth and Planetary Science Letters*, *177*(3–4), 163–176. https://doi.org/10.1016/s0012-821x(00)00055-8

Di Stefano, R., Chiarabba, C., Chiaraluce, L., Cocco, M., De Gori, P., Piccinini, D., & Valoroso, L. (2011). Fault zone properties affecting the rupture evolution of the 2009 (M_w 6.1) L'Aquila earthquake (central Italy): Insights from seismic tomography. *Geophysical Research Letters*, *38*(10), L10310. https://doi.org/10.1029/2011gl047365

Dodge, D. A., Beroza, G. C., & Ellsworth, W. L. (1996). Detailed observations of California foreshock sequences: Implications for the earthquake initiation process. *Journal of Geophysical Research*, *101*(B10), 22371–22392. https://doi.org/10.1029/96jb02269

Ellsworth, W. L., & Beroza, G. C. (1995). Seismic evidence for an earthquake nucleation phase. *Science*, *268*(5212), 851–855. https://doi.org/10.1126/science.268.5212.851

Ellsworth, W. L., & Beroza, G. C. (1998). Observation of the seismic nucleation phase in the Ridgecrest, California, earthquake sequence. *Geophysical Research Letters*, *25*(3), 401–404. https://doi.org/10.1029/97gl53700

Ellsworth, W. L., & Bulut, F. (2018). Nucleation of the 1999 Izmit earthquake by a triggered cascade of foreshocks. *Nature Geoscience*, *11*(7), 531–535. https://doi.org/10.1038/s41561-018-0145-1

Ellsworth, W. L., & Chiaraluce, L. (2009). Supershear during nucleation of the 2009 M 6.3 L'Aquila, Italy earthquake. In *AGU fall meeting abstracts* (Vol. 2009, p. U13C-07).

Eshelby, J. D. (1957). The determination of the elastic field of an ellipsoidal inclusion, and related problems. *Proceedings of the Royal Society of London Series A*, *241*(1226), 376–396.

Essing, D., & Poli, P. (2022). Spatiotemporal evolution of the seismicity in the Alto Tiberina fault system revealed by a high-resolution Template matching catalog. *Journal of Geophysical Research: Solid Earth*, *127*(10), e2022JB024845. https://doi.org/10.1029/2022jb024845

Frank, W. B., Poli, P., & Perfettini, H. (2017). Mapping the rheology of the Central Chile subduction zone with aftershocks. *Geophysical Research Letters*, *44*(11), 5374–5382. https://doi.org/10.1002/2016gl072288

Fujii, Y., & Satake, K. (2007). Tsunami source of the 2004 Sumatra–Andaman earthquake inferred from tide gauge and satellite data. *Bulletin of the Seismological Society of America*, *97*(1A), S192–S207. https://doi.org/10.1785/0120050613

Gvirtzman, S., & Fineberg, J. (2021). Nucleation fronts ignite the interface rupture that initiates frictional motion. *Nature Physics*, *17*(9), 1037–1042. https://doi.org/10.1038/s41567-021-01299-9

Gvirtzman, S., & Fineberg, J. (2023). The initiation of frictional motion-the nucleation dynamics of frictional ruptures. *Journal of Geophysical Research: Solid Earth*, *128*(2), e2022JB025483. https://doi.org/10.1029/2022jb025483

Husseini, M. I., & Randall, M. J. (1976). Rupture velocity and radiation efficiency. *Bulletin of the Seismological Society of America*, *66*(4), 1173–1187. https://doi.org/10.1785/BSSA0660041173

Iio, Y. (1992). Slow initial phase of the P-wave velocity pulse generated by microearthquakes. *Geophysical Research Letters*, *19*(5), 477–480. https://doi.org/10.1029/92gl00179

Iio, Y. (1995). Observations of the slow initial phase generated by microearthquakes: Implications for earthquake nucleation and propagation. *Journal of Geophysical Research*, *100*(B8), 15333–15349. https://doi.org/10.1029/95jb01150

Iio, Y., Ohmi, S., Ikeda, R., Yamamoto, E., Ito, H., Sato, H., et al. (1999). Slow initial phase generated by microearthquakes occurring in the western Nagano Prefecture, Japan-The source effect. *Geophysical Research Letters*, *26*(13), 1969–1972. https://doi.org/10.1029/1999gl900404

INGV Seismological Data Centre. (2006). Rete Sismica Nazionale (RSN). Istituto Nazionale di Geofisica e Vulcanologia (INGV), Italy. https://doi.org/10.13127/SD/X0FXNH7QFY

Kanamori, H. (2004). The diversity of the physics of earthquakes. *Proceedings of the Japan Academy, Series B*, *80*(7), 297–316. https://doi.org/10.2183/pjab.80.297

Kanamori, H., Anderson, D. L., & Heaton, T. H. (1998). Frictional melting during the rupture of the 1994 Bolivian earthquake. *Science*, *279*(5352), 839–842. https://doi.org/10.1126/science.279.5352.839

Kaneko, Y., Nielsen, S. B., & Carpenter, B. M. (2016). The onset of laboratory earthquakes explained by nucleating rupture on a rate-and-state fault. *Journal of Geophysical Research: Solid Earth*, *121*(8), 6071–6091. https://doi.org/10.1002/2016jb013143

Kato, A., Obara, K., Igarashi, T., Tsuruoka, H., Nakagawa, S., & Hirata, N. (2012). Propagation of slow slip leading up to the 2011 M_w 9.0 Tohoku-Oki earthquake. *Science*, *335*(6069), 705–708. https://doi.org/10.1126/science.1215141

Kilb, D., & Gomberg, J. (1999). The initial subevent of the 1994 Northridge, California, earthquake: Is earthquake size predictable? *Journal of Seismology*, *3*(4), 409–420. https://doi.org/10.1023/a:1009890329925

Lapusta, N., & Rice, J. R. (2003). Nucleation and early seismic propagation of small and large events in a crustal earthquake model. *Journal of Geophysical Research*, *108*(B4), ESE8. https://doi.org/10.1029/2001jb000793

Latour, S., Schubnel, A., Nielsen, S., Madariaga, R., & Vinciguerra, S. (2013). Characterization of nucleation during laboratory earthquakes. *Geophysical Research Letters*, *40*(19), 5064–5069. https://doi.org/10.1002/grl.50974

Lucente, F. P., De Gori, P., Margheriti, L., Piccinini, D., Di Bona, M., Chiarabba, C., & Agostinetti, N. P. (2010). Temporal variation of seismic velocity and anisotropy before the 2009 M_w 6.3 L'Aquila earthquake, Italy. *Geology*, *38*(11), 1015–1018. https://doi.org/10.1130/g31463.1

Luzi, L., Lanzano, G., Felicetta, C., D'Amico, M. C., Russo, E., Sgobba, S., et al. (2020). *Engineering strong motion database (ESM) (version 2.0)*. Istituto Nazionale di Geofisica e Vulcanologia (INGV). https://doi.org/10.13127/ESM.2

Madariaga, R., Ruiz, S., Rivera, E., Leyton, F., & Baez, J. C. (2019). Near-field spectra of large earthquakes. *Pure and Applied Geophysics*, *176*(3), 983–1001. https://doi.org/10.1007/s00024-018-1983-x

McLaskey, G. C. (2019). Earthquake initiation from laboratory observations and implications for foreshocks. *Journal of Geophysical Research: Solid Earth*, *124*(12), 12882–12904. https://doi.org/10.1029/2019jb018363

MedNet Project Partner Institutions. (1990). Mediterranean Very Broadband Seismographic Network (MedNet). Istituto Nazionale di Geofisica e Vulcanologia (INGV). https://doi.org/10.13127/SD/FBBBTDTD6Q

Mori, J., & Kanamori, H. (1996). Initial rupture of earthquakes in the 1995 Ridgecrest, California sequence. *Geophysical Research Letters*, *23*(18), 2437–2440. https://doi.org/10.1029/96gl02491

Ohnaka, M. (2000). A physical scaling relation between the size of an earthquake and its nucleation zone size. *Pure and Applied Geophysics*, *157*(11), 2259–2282. https://doi.org/10.1007/pl00001084

Ohnaka, M., & Shen, L. F. (1999). Scaling of the shear rupture process from nucleation to dynamic propagation: Implications of geometric irregularity of the rupturing surfaces. *Journal of Geophysical Research*, *104*(B1), 817–844. https://doi.org/10.1029/1998jb900007

Passelègue, F. X., Almakari, M., Dublanchet, P., Barras, F., Fortin, J., & Violay, M. (2020). Initial effective stress controls the nature of earthquakes. *Nature Communications*, *11*(1), 1–8. https://doi.org/10.1038/s41467-020-18937-0

Peng, Z., & Zhao, P. (2009). Migration of early aftershocks following the 2004 Parkfield earthquake. *Nature Geoscience*, *2*(12), 877–881. https://doi.org/10.1038/ngeo697

Poli, P., Marguin, V., Wang, Q., d'Agostino, N., & Johnson, P. (2020). Seasonal and coseismic velocity variation in the region of L'Aquila from single station measurements and implications for crustal rheology. *Journal of Geophysical Research: Solid Earth*, *125*(7), e2019JB019316. https://doi.org/10.1029/2019jb019316

Poli, P., Prieto, G., Rivera, E., & Ruiz, S. (2016). Earthquakes initiation and thermal shear instability in the Hindu Kush intermediate depth nest. *Geophysical Research Letters*, *43*(4), 1537–1542. https://doi.org/10.1002/2015gl067529

Poli, P., & Prieto, G. A. (2016). Global rupture parameters for deep and intermediate-depth earthquakes. *Journal of Geophysical Research: Solid Earth*, *121*(12), 8871–8887. https://doi.org/10.1002/2016jb013521

Rubinstein, S. M., Cohen, G., & Fineberg, J. (2004). Detachment fronts and the onset of dynamic friction. *Nature*, *430*(7003), 1005–1009. https://doi.org/10.1038/nature02830

Ruiz, S., Aden-Antoniow, F., Baez, J. C., Otarola, C., Potin, B., Del Campo, F., et al. (2017). Nucleation phase and dynamic inversion of the M_w 6.9 Valparaíso 2017 earthquake in Central Chile. *Geophysical Research Letters*, *44*(20), 10–290. https://doi.org/10.1002/2017GL075675

Ruiz, S., Metois, M., Fuenzalida, A., Ruiz, J., Leyton, F., Grandin, R., et al. (2014). Intense foreshocks and a slow slip event preceded the 2014 Iquique M_w 8.1 earthquake. *Science*, *345*(6201), 1165–1169. https://doi.org/10.1126/science.1256074

Sallarès, V., & Ranero, C. R. (2019). Upper-plate rigidity determines depth-varying rupture behaviour of megathrust earthquakes. *Nature*, *576*(7785), 96–101. https://doi.org/10.1038/s41586-019-1784-0

Sánchez-Reyes, H., Essing, D., Beaucé, E., & Poli, P. (2021). The imbricated foreshock and aftershock activities of the Balsorano (Italy) M_w 4.4 normal fault earthquake and implications for earthquake initiation. *Seismological Research Letters*, *92*(3), 1926–1936. https://doi.org/10.1785/0220200253

Savage, M. K. (2010). The role of fluids in earthquake generation in the 2009 M_w 6.3 L'Aquila, Italy, earthquake and its foreshocks. *Geology*, *38*(11), 1055–1056. https://doi.org/10.1130/focus112010.1

Scognamiglio, L., Tinti, E., Michelini, A., Dreger, D. S., Cirella, A., Cocco, M., et al. (2010). Fast determination of moment tensors and rupture history: What has been learned from the 6 April 2009 L'Aquila earthquake sequence. *Seismological Research Letters*, *81*(6), 892–906. https://doi.org/10.1785/gssrl.81.6.892

Scuderi, M. M., & Collettini, C. (2016). The role of fluid pressure in induced vs. triggered seismicity: Insights from rock deformation experiments on carbonates. *Scientific Reports*, *6*(1), 1–9. https://doi.org/10.1038/srep24852

Shibazaki, B., & Matsu'ura, M. (1998). Transition process from nucleation to high-speed rupture propagation: Scaling from stick-slip experiments to natural earthquakes. *Geophysical Journal International*, *132*(1), 14–30. https://doi.org/10.1046/j.1365-246x.1998.00409.x

Tape, C., Holtkamp, S., Silwal, V., Hawthorne, J., Kaneko, Y., Ampuero, J. P., et al. (2018). Earthquake nucleation and fault slip complexity in the lower crust of central Alaska. *Nature Geoscience*, *11*(7), 536–541. https://doi.org/10.1038/s41561-018-0144-2

Terakawa, T., Zoporowski, A., Galvan, B., & Miller, S. A. (2010). High-pressure fluid at hypocentral depths in the L'Aquila region inferred from earthquake focal mechanisms. *Geology*, *38*(11), 995–998. https://doi.org/10.1130/g31457.1

Trasatti, E., Kyriakopoulos, C., & Chini, M. (2011). Finite element inversion of DInSAR data from the M_w 6.3 L'Aquila earthquake, 2009 (Italy). *Geophysical Research Letters*, *38*(8), L08306. https://doi.org/10.1029/2011gl046714

Trugman, D. T., & Shearer, P. M. (2017). GrowClust: A hierarchical clustering algorithm for relative earthquake relocation, with application to the Spanish Springs and Sheldon, Nevada, earthquake sequences. *Seismological Research Letters*, *88*(2A), 379–391. https://doi.org/10.1785/0220160188

Umeda, Y. (1990). High-amplitude seismic waves radiated from the bright spot of an earthquake. *Tectonophysics*, *175*(1–3), 81–92. https://doi.org/10.1016/0040-1951(90)90131-q

Valoroso, L., Chiaraluce, L., Piccinini, D., Di Stefano, R., Schaff, D., & Waldhauser, F. (2013). Radiography of a normal fault system by 64,000 high-precision earthquake locations: The 2009 L'Aquila (central Italy) case study. *Journal of Geophysical Research: Solid Earth*, *118*(3), 1156–1176. https://doi.org/10.1002/jgrb.50130

Venkataraman, A., & Kanamori, H. (2004). Observational constraints on the fracture energy of subduction zone earthquakes. *Journal of Geophysical Research*, *109*(B5), B05302. https://doi.org/10.1029/2003jb002549

Walter, W. R., Yoo, S. H., Mayeda, K., & Gök, R. (2017). Earthquake stress via event ratio levels: Application to the 2011 and 2016 Oklahoma seismic sequences. *Geophysical Research Letters*, *44*(7), 3147–3155. https://doi.org/10.1002/2016gl072348